Realistic models of paracrystalline silicon

S. M. Nakhmanson*
Department of Physics and Astronomy and CMSS, Ohio University, Athens, Ohio 45701

P. M. Voyles†
Department of Physics, University of Illinois, 1110 West Green St., Urbana, Illinois 61801
and NEC Research Institute, 4 Independence Way, Princeton, New Jersey 08540

Normand Mousseau‡
Department of Physics and Astronomy and CMSS, Ohio University, Athens, Ohio 45701

G. T. Barkema§
Theoretical Physics, Utrecht University, Princetonplein 5, 3584 CC Utrecht, the Netherlands

D. A. Drabold‖
Department of Physics and Astronomy and CMSS, Ohio University, Athens, Ohio 45701
(Received 2 January 2001; published 31 May 2001)

We present a procedure for the preparation of physically realistic models of paracrystalline silicon based on a modification of the bond-switching method of Wooten, Winer, and Weaire. The models contain randomly oriented *c*-Si grains embedded in a disordered matrix. Our technique creates interfaces between the crystalline and disordered phases of Si with an extremely low concentration of coordination defects. The resulting models possess structural and vibrational properties comparable with those of good continuous random network models of amorphous silicon and display realistic optical properties, correctly reproducing the electronic band gap of amorphous silicon. The largest of our models also shows the best agreement of any atomistic model structure that we tested with fluctuation microscopy experiments, indicating that this model has a degree of medium-range order closest to that of the real material.

DOI: 10.1103/PhysRevB.63.235207 PACS number(s): 61.43.Dq, 71.55.Jv, 61.20.Ja

I. INTRODUCTION

Recent fluctuation electron microscopy (FEM) experiments have shown signatures of medium-range order (MRO) in as-deposited amorphous semiconductor thin films.[1,2] These results have been interpreted as indicating the presence in the amorphous films of small (<30 Å) topologically crystalline grains, which are distorted by strain and embedded in a disordered matrix. Such material is called paracrystalline.[2] It has the structure factor of amorphous material, but nonetheless has significant MRO. It is difficult to verify this interpretation by other experimental techniques, so computer modeling has been used to study the structure of these complex systems and the traces of MRO in them. In this paper we present large scale atomistic models of paracrystalline Si that are electronically realistic. Simulated FEM on these models reproduces the experimental measurements more accurately than any other model tested.

Only a model that agrees with a whole set of experiments, including structural, optical, and vibrational characterizations, can reliably describe a real material. One of the most common methods for constructing continuous random network (CRN) models of *a*-Si, the molecular dynamics (MD) ''quench from the melt'' procedure, does not meet this criterion, as it produces models with relatively poor electronic properties. The best large (1000 atoms and more) models created with this technique[3] tend to have at least 3–4 % concentration of coordination defects, as well as significant residual network strain, which manifests itself as an increased width of the bond-angle distribution $\Delta\theta$ compared to the experimental value.[4] The electronic states associated with these structural defects fill out the optical gap of the model material,[5,6] essentially turning the model from a semiconductor into a poor metal.[7] This is clearly unphysical. However, these models can have a reasonable phonon spectrum and pair-correlation function, which can be misleading, since the results of simulations with these models involving their electronic properties cannot be fully trusted.

The only family of models of paracrystalline Si previously available was a set of models developed by Keblinski *et al.*[2,8] using empirical MD with the Stillinger-Weber potential[9] and a ''quench from the melt'' procedure in which *c*-Si grains are introduced into the melt and not allowed to dissolve.[10] Recently, these authors and others have extensively studied the properties of these models[8] and found that, like CRN models produced in a similar way, these paracrystalline models have an unphysically high density of defect electron states in the band gap region. They do, however, better reproduce the degree of MRO present in experimentally grown *a*-Si films[2] than a variety of CRN models. Our challenge was therefore to create a model that would comply with all the experiments simultaneously. In order to do that we have employed the bond-switching algorithm of Wooten, Winer, and Weaire[11] (WWW), modified by Barkema and Mousseau,[12] which produces the best current CRN models. The original WWW method was used by Nomura *et al.*[13] to

study electronic properties of nanocrystallites in *a*-Si but for unknown reasons produced poor results.

II. MODEL PREPARATION

In the method of Barkema and Mousseau, atoms are randomly placed into a cubic box with periodic boundary conditions at crystalline density, subject to the condition that no two atoms are too close together. The atoms are then connected by ''artificial'' bonds in such a way that a perfectly tetravalent network is created. These bonds exist only in the form of a neighbor list constructed for each atom, so they can be unphysically long. The network is subjected to a large number of bond-switching transpositions followed by local structural rearrangements which result in a highly relaxed, low-strain configuration.

We generally follow this procedure to create paracrystalline models, but before filling the box with atoms we position inside it one or more crystalline grains, randomly oriented with respect to one another. The grains are created by starting with a spherical section of crystalline Si and keeping only those atoms that have two and more nearest neighbors which also belong to the grain. For reasons described below we also require the grain to contain an even number of atoms that have three nearest neighbors.

When the grain is positioned inside the box, a nearest neighbor list is created for it and the two- and three fold coordinated atoms on the surface are identified. After the grains are set in place the remaining volume is randomly seeded with ''matrix'' atoms, which are then connected into a perfectly fourfold network. The grains are at this point disconnected from the disordered matrix and need to be incorporated into it in such a way that all the atoms have exactly four nearest neighbors. This is done in two steps. First, for any twofold grain atom the closest bonded pair of matrix atoms is found, the bond between the matrix atoms is broken, and two new bonds between each of the matrix atoms and the grain atom are formed. Second, for each threefold grain atom the closest additional threefold grain atom is found, then the bonded pair of matrix atoms closest to both threefold grain atoms is found, and the bond between these atoms is broken and two new threefold grain atom/matrix atom bonds are formed. This requires an even number of three-fold grain atoms. This algorithm creates a number of unphysically long bonds, but these high-energy bonds are sure to be broken during the bond-switching transpositions.

After the perfectly fourfold network containing both the crystalline grains and the matrix is constructed, it is subjected to bond-switching moves in order to minimize the system's energy. Unlike in the WWW method, we constrain the bond switching in order to preserve the crystalline topology of the grains during energy minimization. Bonds between grain atoms are not allowed to break; only bonds between a grain atom and a matrix atom or between two matrix atoms can be broken. An additional constraint is imposed on the positions of the grain atoms: during the initial phase of the relaxation, while strain in the system is relatively high, the coordinates of the grain atoms are fixed. When the energy of the system with fixed grain atoms reaches its minimum, the grain atoms are allowed to move and the energy is minimized again.

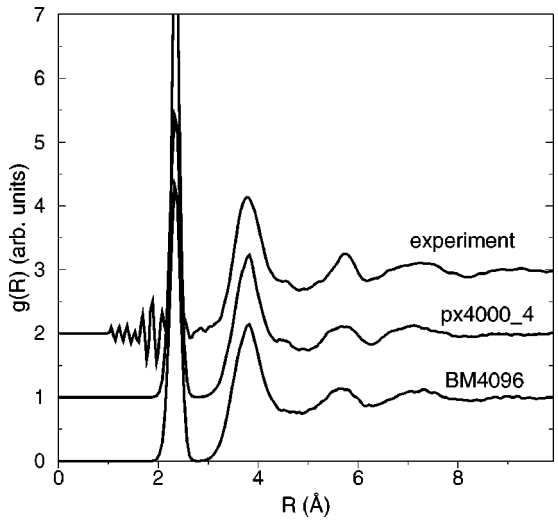

FIG. 1. Radial-distribution function $g(R)$ for 4000-atom paracrystalline model and 4096-atom CRN model. The experimental curve is taken from Ref. 4.

III. DISCUSSION OF RESULTS

A. Structure and vibrational properties

Using the procedure described in the previous section we have constructed three models of paracrystalline silicon. The first 400-atom model, called px400, has one grain consisting of 44 atoms, positioned in the center of a 20 Å cubic box. This model was created mostly for testing purposes. The second model, px1000, has 1000 atoms, of which 86 belong to a single grain placed in the center of a cubic box with a side of approximately 28 Å. The third 4000-atom model, px4000_4, has four crystalline grains of roughly the same size (100 atoms), randomly oriented with respect to one another and positioned at the vertices of a tetrahedron the center of which lies at the center of the 43 Å cubic supercell. The two smaller models are 100% fourfold coordinated while the largest one has eight fivefold and two sixfold coordinated atoms. All the models have $\Delta\theta < 10.6°$, which is in excellent agreement with experiment.

The radial-distribution function $g(R)$ for our largest model px4000_4 is presented in Fig. 1. The curve computed for a 4096-atom CRN model of Barkema and Mousseau,[12] BM4096, and the experimental curve[4] are shown for comparison. The curves for the models look almost exactly the same and both seem to be in very good agreement with the experimental data.

The bond-angle θ and the dihedral-angle ϕ distributions for px4000_4 and BM4096 are presented in Fig. 2. The bond-angle distributions for both models look identical while the dihedral-angle distribution for the paracrystalline model has a pronounced peak at 60° which is not present in the distribution for the CRN model. This feature is explained by the fact that compared to the CRN the paracrystalline model has a larger share of atoms (mostly the ones belonging to the

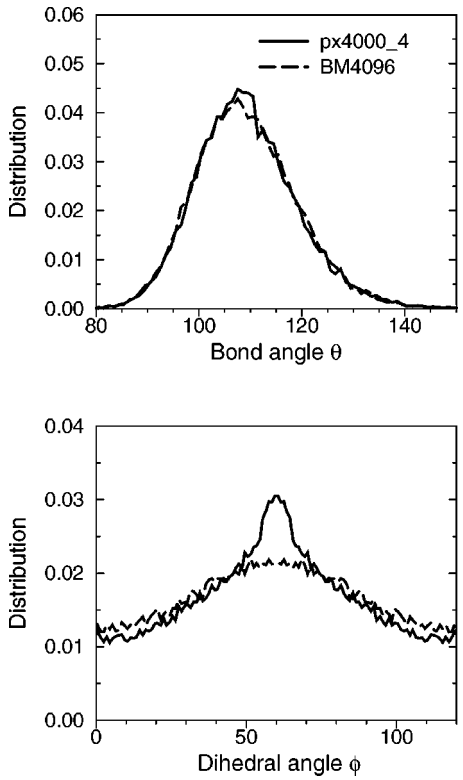

FIG. 2. Bond-angle (upper panel) and dihedral-angle (lower panel) distributions for 4000-atom paracrystalline and 4096-atom CRN models.

central regions of the grains) whose local environment is very close to crystalline, thus favoring $\phi = 60°$. We should note, however, that the total number of such atoms is an order of magnitude lower than the number of disordered atoms in the model, which makes the bond-angle distributions for the paracrystalline and CRN models look almost identical. An important point regarding the calculation of dihedral-angle distribution (or any other correlation function of the same or higher order) is that except for the FEM simulations (see below) it is the only nontopological way to distinguish between CRN and paracrystalline structures.

The vibrational density of states (VDOS) curves for px4000_4 and a 1000-atom CRN model of Barkema and Mousseau, called BM1000 here, are shown in Fig. 3. The results for two smaller paracrystalline models are not presented because their VDOS curves are almost identical to that of the largest model. The curves for both models shown in the figure look very similar as well. The VDOS for all the models has been calculated by a direct diagonalization of their dynamical matrices computed with the modified Stillinger-Weber potential.[14] Prior to the dynamical matrix calculation the models were relaxed with a simulated MD quench employing the same potential.

B. Electronic properties

In the upper panel of Fig. 4, we present the band gap region of the electronic density of states (EDOS) of px400, px1000, and BM1000. The total EDOS is shown in the inset;

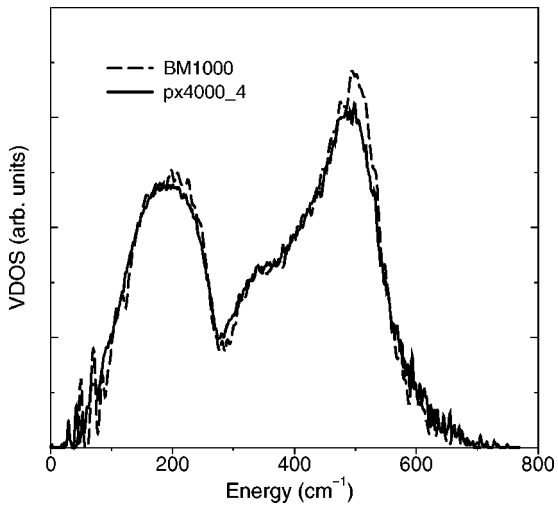

FIG. 3. The VDOS's for 4000-atom paracrystalline and 1000-atom CRN models.

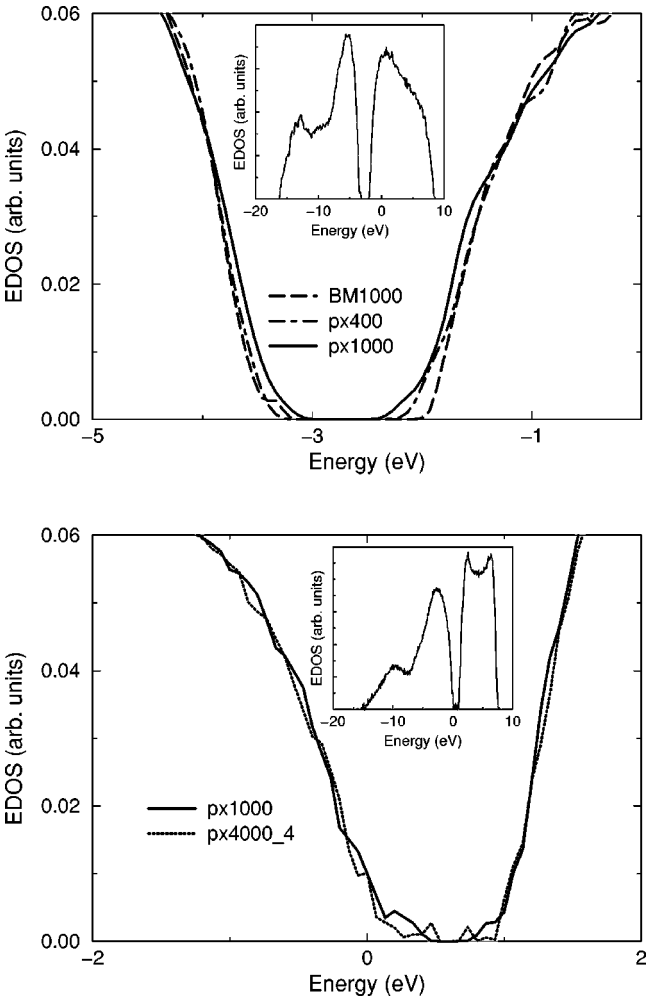

FIG. 4. The band gap region of the EDOS calculated with local-basis *ab initio* method for 400- and 1000-atom models (upper panel) and with empirical tight-binding Hamiltonian for 1000- and 4000-atom models (lower panel). The total EDOS is shown on the panel inserts.

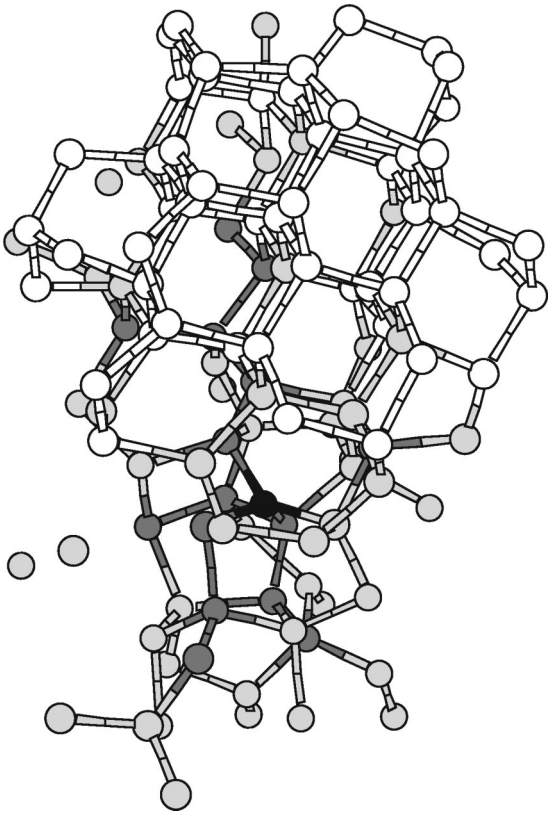

FIG. 5. Electronic band gap state localized on the grain boundary. The black atom accounts for more than 20% of the total electron charge. Each atom pictured in dark gray accounts for between 1% and 10%, and each light gray atom accounts for between 0.1% and 1%. The white atoms are all of the other atoms in the grain.

at this scale it is indistinguishable for all three models. The EDOS for all these models has been calculated with the FIREBALL local-basis *ab initio* code.[15] In the lower panel of Fig. 4, the band gap region for the EDOS of px4000_4 computed with empirical tight-binding Hamiltonian of Kwon *et al.*[16] is shown. The total EDOS for px4000_4 is presented in the inset to the lower panel. The EDOS band gap region curve for px1000 calculated with the same method is also shown for reference—note how the empirical tight-binding calculation tends to underestimate the band gap compared to the more advanced *ab initio* method. We must point out that, of course, both methods produce band gap widths that are quantitatively unrealistic.

We have also studied the nature of the valence band tail and band gap states in our largest model, px4000_4. All of these states are localized, and according to their localization patterns can be divided into two groups of roughly equal size. The states from the first group localize on strained regions of the network in the disordered matrix, which has also been observed for large CRN Si models.[17] The states belonging to the second group are localized on the grain boundaries, which obviously also contain some highly strained bonds. This leads us to believe that in paracrystalline Si the grain boundaries are electrically active, and that the electronic states localized on them govern the valence band tail behavior of the material. An example of a valence band tail state localized at a paracrystalline boundary is shown in Fig 5. Figure 5 also shows the topologically crystalline nature of the grain, retained by construction during the model preparation.

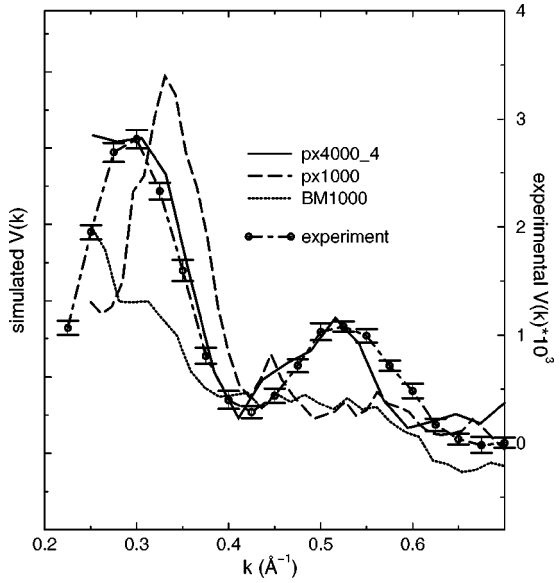

FIG. 6. Simulated fluctuation microscopy signal $V(k)$ for the models, and experimental measurements for a sputtered a-Si thin film, all at 15 Å resolution.

C. Medium range order

We have computed the fluctuation microscopy signal $V(k)$ for the models, shown in Fig. 6 with experimental data from a sputtered a-Si thin film.[18] $V(k)$ is the normalized variance of mesoscopic-resolution hollow-cone dark-field (HCDF) transmission electron micrographs as a function of the dark-field scattering vector magnitude k.[1] A large $V(k)$ with significant structure in k indicates that the sample has significant MRO; a small $V(k)$ with little structure indicates that the sample has little or no MRO.[19] Quantitatively, $V(k)$ depends on the three- and four-body atom distribution functions of the sample.[20]

$V(k)$ for the models is found by computing the variance of a series of simulated HCDF images of the model. Each HCDF image is built up from many coherent tilted dark-field (TDF) images. The TDF images were computed in the phase-grating approximation,[21] which approximates the sample with a transmission function that is just the potential of the sample projected along the direction of travel of the electron beam. For a crystalline lattice of the same size as the models studied here, this would be inadequate, since it ignores effects such as dynamical scattering and electron channeling. However, these effects are greatly suppressed in the absence of a crystalline lattice. The TDF image intensity is the squared modulus of the incident wave multiplied by the transmission function and then convolved with the microscope point-spread function. To compute the intensity for an incoherently filled hollow-cone annulus of finite width, we sum the TDF image intensities for many incoming wave vectors inside the annulus. In an effort to better approach an

ensemble average of structures, we compute HCDF images for each model in a large number of orientations for each k. This is equivalent to assuming that the grain orientations are uncorrelated, which is also assumed in the model preparation. Images were computed at a resolution of 15 Å to match the resolution used in the experiment.

Despite the use of the phase-grating approximation, there are residual effects in $V(k)$ from the different number of unique atoms in the models. These have been corrected using a variation on the empirical thickness correction technique developed for a-Si thin film experimental measurements.[22] The thickness correction expression contains a parameter that allows for the formation of a surface oxide on the thin foil; that parameter has been set to zero for these calculations since the models have no oxide.

The raw simulated $V(k)$ is larger than the measured variance by approximately an order of magnitude. This is due to several effects, the first of which is the small size of the models (at most 43 Å) compared to the thickness of the experimental samples, which is $\sim$200 Å. The empirical thickness correction cannot fully correct for this because the experimentally determined fitting parameters employed are not sufficiently accurate, making the procedure unreliable for large thickness corrections. It has been employed in the experiments to correct for small thickness perturbations; it is used here in the same spirit to make the models comparable to one another. The experimental images are also bandpass filtered to remove experimental artifacts associated with sample nonuniformities, but the simulated images are too small for this treatment. The simulations also do not account for several sources of small-angle scattering, including inelastic scattering, multiple scattering, and thermal diffuse scattering, which are present to some degree in the experimental measurement, and will tend to reduce the image variance. All of these effects (thickness, filtering, and small-angle scattering) are k independent, so in Fig. 6 we have simply scaled all the data by a multiplicative factor to get the best match to the experimental data for the best model, which is px4000_4 (see below). We then interpret the simulations only in terms of the positions and relative magnitudes of features in $V(k)$.

$V(k)$ for BM1000 shows the nearly featureless $V(k)$ that is typical of CRN models.[2,8] px1000 shows the prominent peak at $k=0.3$ Å^{-1} that is observed in the experiment and is a measurable signature of paracrystallinity. It does not fully reproduce the second peak at $k=0.55$ Å^{-1} seen in the data, most likely because it has only one grain and a very small degree of MRO. The simulated $V(k)$ curve for our largest model, px4000_4, presents the best match currently available to the experiment: the simulated $V(k)$ closely follows the shape of the experimental curve and correctly reproduces the ratio of the first to the second peak heights and positions of both peaks.

It is unlikely that the combination of grain size, density, shape, spatial distribution, and orientation distribution in px4000_4 is unique in producing a $V(k)$ with this level of agreement with experiment. Further simulations are required to explore the effects of all these parameters on the shape and magnitude of $V(k)$. Improved $V(k)$ simulations should also bring the simulated magnitude closer to the experimental value.

IV. CONCLUSIONS

To summarize, we have created a family of models for paracrystalline Si that not only have structural MRO in qualitative agreement with experiment, but also have realistic vibrational, structural, and optical properties. The EDOS band gaps are comparable in width with the gap for the best CRN models for a-Si. Except for measurements focused directly on the medium-range order, it is essentially impossible to distinguish between the amorphous and the paracrystalline models.

The evidence presented here shows that our current models can serve as a reasonable description for tetravalent, paracrystalline, semiconducting material and as testing grounds for other measurements of medium-range order in disordered semiconductors.

ACKNOWLEDGMENTS

This work was supported by NSF under Grants No. DMR 00-81006 (S.M.N. and D.A.D.), No. DMR 98-05848, (N.M.) and No. DMR 97-03906 (P.M.V.). We thank J. M. Gibson for the use of his fluctuation microscopy simulation code and J. R. Abelson and J. E. Gerbi for providing the sample from which the experimental data were taken.

*Present address: Department of Physics, North Carolina State University, Raleigh, North Carolina 27695. Email address: nakhmans@nemo.physics.ncsu.edu

†Current address: Bell Laboratories, Lucent Technologies, Murray Hill, NJ 07974. Email address: pvoyles@bell-labs.com

‡Email address: mousseau@helios.phy.ohiou.edu

§Email address: barkema@phys.uu.nl

‖Email address: drabold@ohiou.edu

[1] M.M.J. Treacy and J.M. Gibson, Acta Crystallogr., Sect. A: Found. Crystallogr. **52**, 212 (1996).

[2] M.M.J. Treacy, J.M. Gibson, and P.J. Keblinski, J. Non-Cryst. Solids **231**, 99 (1998).

[3] J.F. Justo, M.Z. Bazant, E. Kaxiras, V.V. Bulatov, and S. Yip, Phys. Rev. B **58**, 2539 (1998).

[4] K. Laaziri, S. Kycia, S. Roorda, M. Chicoine, J.L. Robertson, J. Wang, and S.C. Moss, Phys. Rev. B **60**, 13 520 (1999).

[5] R. Biswas, C.Z. Wang, C.T. Chan, K.M. Ho, and C.M. Soukoulis, Phys. Rev. Lett. **63**, 1491 (1989).

[6] M. Fornari, M. Peressi, S. de Gironcoli, and A. Baldereschi, Europhys. Lett. **47**, 481 (1999).

[7] The electronic density of states of the model, presented in Ref. 3 has been recently calculated by N. Bernstein, M.J. Mehl, D.A. Papaconstantopoulos, N.I. Papanicolaou, R.Z. Bazant, and E. Kaxiras, Phys. Rev. B **62**, 4477 (2000).

[8] P. M. Voyles, N. Zotov, S. M. Nakhmanson, D. A. Drabold, J. M. Gibson, M. M. J. Treacy, and P. Keblinski (unpublished).

[9] F.H. Stillinger and T.A. Weber, Phys. Rev. B **31**, 5262 (1985).

[10] P. Keblinski, S.R. Phillpot, D. Wolf, and H. Gleiter, Acta Mater.

45, 987 (1997).
[11] F. Wooten, K. Winer, and D. Weaire, Phys. Rev. Lett. **54**, 1392 (1985).
[12] G.T. Barkema and N. Mousseau, Phys. Rev. B **62**, 4985 (2000).
[13] S. Nomura, X.W. Zhao, Y. Aoyagi, and T. Sugano, *et al.*, Phys. Rev. B **54**, 13 974 (1996); S. Nomura T. Iitaka, X. Zhao, T. Sugano, and Y. Aoyagi, Mater. Sci. Eng., B **51**, 146 (1998).
[14] R. L. C. Vink, G. T. Barkema, W. F. van der Weg and N. Mousseau (unpublished).
[15] O.F. Sankey and D.J. Niklewski, Phys. Rev. B **40**, 3979 (1989); O.F. Sankey, D.A. Drabold, and G.B. Adams, Bull. Am. Phys. Soc. **36** (8), 924 (1991).
[16] I. Kwon, R. Biswas, C.Z. Wang, K.M. Ho, and C.M. Soukoulis, Phys. Rev. B **49**, 7242 (1994).
[17] J. Dong and D.A. Drabold, Phys. Rev. Lett. **80**, 1928 (1998).
[18] P. M. Voyles, J. E. Gerbi, M. M. J. Treacy, J. M. Gibson, and J. R. Abelson (unpublished).
[19] P.M. Voyles, J.M. Gibson, and M.M.J. Treacy, J. Electron Microsc. **49**, 259 (2000).
[20] J.M. Gibson, M.M.J. Treacy, and P.M. Voyles, Ultramicroscopy **83**, 169 (2000).
[21] See, e.g., E. J. Kirkland, *Advanced Computing in Electron Microscopy* (Plenum Press, New York, 1998), pp. 63–97.
[22] P. M. Voyles, M. M. J. Treacy, J. M. Gibson, H-C. Jin, and J. R. Abelson, in *Materials Problem Solving with the Electron Microscope*, edited by J. Bentley, V. Dahmen, C. Allen, and I. Petrov, MRS Symposia Proceedings NO. 589 (Materials Research Society, Pittsburgh, in press).